

The British University in Egypt

BUE Scholar

Nanotechnology Research Centre

Research Centres of Excellence

11-2024

Decorating carbon nanotubes with different ratios of graphene quantum dots via ultrasonication as a potential material for CO₂ capture

Mohamed Morsy
mohamed.morsy@bue.edu.eg

Follow this and additional works at: https://buescholar.bue.edu.eg/nanotech_research_centre

Recommended Citation

Morsy, Mohamed, "Decorating carbon nanotubes with different ratios of graphene quantum dots via ultrasonication as a potential material for CO₂ capture" (2024). *Nanotechnology Research Centre*. 120. https://buescholar.bue.edu.eg/nanotech_research_centre/120

This Article is brought to you for free and open access by the Research Centres of Excellence at BUE Scholar. It has been accepted for inclusion in Nanotechnology Research Centre by an authorized administrator of BUE Scholar. For more information, please contact bue.scholar@gmail.com.



Decorating carbon nanotubes with different ratios of graphene quantum dots via ultrasonication as a potential material for CO₂ capture

Mohamed Morsy, Ahmed Helal, Islam Gomaa, Sabah M. Abdelbasir & Ahmed Maysara

To cite this article: Mohamed Morsy, Ahmed Helal, Islam Gomaa, Sabah M. Abdelbasir & Ahmed Maysara (2024) Decorating carbon nanotubes with different ratios of graphene quantum dots via ultrasonication as a potential material for CO₂ capture, HBRC Journal, 20:1, 58-73, DOI: [10.1080/16874048.2024.2422746](https://doi.org/10.1080/16874048.2024.2422746)

To link to this article: <https://doi.org/10.1080/16874048.2024.2422746>



© 2024 The Author(s). Published by Informa UK Limited, trading as Taylor & Francis Group.



Published online: 08 Nov 2024.



Submit your article to this journal [↗](#)



Article views: 11



View related articles [↗](#)



View Crossmark data [↗](#)

Decorating carbon nanotubes with different ratios of graphene quantum dots via ultrasonication as a potential material for CO₂ capture

Mohamed Morsy^{a,b}, Ahmed Helal^c, Islam Gomaa^b, Sabah M. Abdelbasir^c and Ahmed Maysara^b





^aBuilding Physics and Environment Institute, Housing & Building National Research Center (HBRC), Giza, Egypt; ^bNanotechnology Research Centre (NTRC), The British University in Egypt (BUE), Cairo, Egypt; ^cNanostructured Materials and Nanotechnology Division, Central Metallurgical Research and Development Institute, Cairo, Egypt

ABSTRACT

The harmful impacts of carbon dioxide (CO₂) emissions are represented mainly in global warming as a major greenhouse gas, health problem issues, and pollution. As a result, there is currently worldwide interest in developing efficient adsorbents with high adsorption capacity for CO₂ gas. In this work, the adsorbent nanocomposites were synthesized from different loadings of graphene quantum dots (10, 20, and 30%) with carbon nanotubes (CNTs) using the ultrasonication method. The prepared nanocomposites were characterized by XRD, HR-TEM UV-Vis, Raman, and BET, techniques to investigate their chemical and physical characteristics. The samples reveal a high surface area and porosity. The optical band gap was calculated for the nanocomposites; it decreased upon increasing the ratio of the QDs, since the 30% QDs/CNT show an E_g of about 1.93 eV compared to 2.1 eV for the 10% and 20% QDs/CNTs. The samples of 20% and 30% QDs/CNTs revealed the highest active site density; furthermore, they showed the best performance for CO₂ gas capture of about 24.6 mmol. g⁻¹ and 25 mmol. g⁻¹, which makes these nanocomposites efficient adsorbents for CO₂ emissions.

ARTICLE HISTORY Received 9 May 2024; Revised 2 October 2024; Accepted 16 October 2024

KEYWORDS Carbon nanomaterials; QDs; Nanocomposites; CO₂ capture; XRD of carbon nanotubes; HR-TEM

CONTACT Mohamed Morsy  83morsy@gmail.com  Building Physics and Environment Institute, Housing & Building National Research Center (HBRC), Dokki, Giza 12311, Egypt; Ahmed Helal  ahelal31@yahoo.com  Nanotechnology Research Centre (NTRC), The British University in Egypt (BUE), Cairo, Egypt

© 2024 The Author(s). Published by Informa UK Limited, trading as Taylor & Francis Group.
This is an Open Access article distributed under the terms of the Creative Commons Attribution-NonCommercial License (<http://creativecommons.org/licenses/by-nc/4.0/>), which permits unrestricted non-commercial use, distribution, and reproduction in any medium, provided the original work is properly cited. The terms on which this article has been published allow the posting of the Accepted Manuscript in a repository by the author(s) or with their consent.

Introduction

Under normal atmospheric conditions, carbon dioxide is colorless, nonflammable, and less abundant than oxygen and nitrogen in the surrounding atmosphere. The importance of carbon dioxide comes from its ability to keep our planet warm. Its concentrations are in the range of 400 ppm and 270 ppm after and before human industrial activity [1]. The emission of carbon dioxide in the atmosphere has increased rapidly due to the industrial revolution. The harmful impacts of carbon dioxide emissions are represented mainly in global warming, health problem issues, and pollution [2]. Different heavy industries such as mining, automobile manufacturing, steel, and cement industries release huge quantities of carbon dioxide into the air [3,4]. To realize the emitted amount of carbon dioxide in the atmosphere we can imagine that each ton of cement produces approximately 800 kg of carbon dioxide. Going forward from its harmful effects on both human beings and the environment, CO₂ capture is not a luxury, it requires great attention from academia and industrial policymakers [5]. The CO₂ capture can be executed through different strategies including physical adsorption by solids, chemical absorption by amine solutions, cryogenic distillation, and membrane separation [6,7]. CO₂ capture by amine solutions is used commercially, however some disadvantages related to cost, equipment corrosion, or degradation of the solvent were encountered, thereby physical adsorption is an alternative [8]. Different functional materials including but not limited to metal organic framework (MOF) [9], polymers, zeolite, fly ash, silica, and carbon nanomaterials were recommended and studied as a potential candidate for CO₂ capture [10].

The nanocarbon-based materials are made up of carbon with varied morphology on nanoscale. These materials comprise 0D, 1D, 2D, and 3D nanostructures such as graphene quantum dots (GQDs), carbon nanotubes (CNTs), graphene (G), and graphene foam (GF), respectively [11–13]. In addition to the most common properties of carbon nanomaterials, CNTs are characterized by hollow structures in addition to the ability of attaching different functional groups on its surface through chemical or thermal treatment [14,15]. One of the most recently examined members of the carbon nanomaterials for CO₂ capture is GQDs. GQDs are 0D nanoparticles having a size less than 10 nm [16]. It has a good reputation in scientific media as it shows a promising attitude in many applications. GQDs have a potential application in photocatalysis [17], electrocatalysis, optoelectronic devices, biomedical applications [18], supercapacitors [19], and CO₂ adsorption [20] due to low toxicity, biocompatibility, stability, adjustable optical and electrical properties, and low fabrication cost [21]. Among synthesized methods of GQDs [22], the hydrothermal route is the most popular one due to the high yield, low production cost, and low energy

consumption [23]. Recently, Zhu et al fabricated a membrane based on GQDs for CO₂ separation. A new method based on microalgae has been developed by Guo et al for producing two types of carbon materials (carbon quantum dots and porous carbon). They proved the effectiveness of the synthesized structure for cellular imaging and CO₂ capture and reported that the adsorption capacity of 4.2 and 6.9 mmol g⁻¹ at ~1 bar at 298°K and 273 °K, respectively, has been achieved [20]. Smart CO₂-philic membranes for highly efficient CO₂ separation and sensitive online CO₂ detection have been synthesized using optical active GQD@Pebax by Yeh Y-J et.al [24].

The main objective of this work is to investigate the effect of the amount of GQDs loaded over CNTs on the CO₂ capture efficiency. Different amounts of GQDs (10%, 20%, and 30%) were loaded on the external surface of multi-walled carbon nanotubes (MWCNTs) via the ultrasonication method. The properties of the resultant structures were investigated through XRD, HRTEM, UV-Vis, Raman and BET analysis. The earlier mentioned techniques demonstrate the successful decoration of GQDs over the external surface of MWCNTs. The HRTEM proved the successful attachment of GQDs on the external surface of MWCNTs. The average crystallite size of GQDs was estimated from XRD and found about 2 nm. To the best knowledge of the authors, this is the first study that reports CO₂ capture using GQDs/CNTs nanocomposite. The CO₂ capture of 24.6 mmol. g⁻¹ and 25 mmol. g⁻¹ were verified for 20% GQD/CNTs and 30% GQD/CNT with basic site densities of 0.28 and 0.25, respectively, in addition to pore size diameters of 49.6 nm and 52.3 nm, respectively.

Chemicals

Citric acid (C₆H₈O₇, 99.5%), and sodium hydroxide (NaOH, ≥ 97%) were obtained from Fisher Chemical. MWCNTs were synthesized using atmospheric pressure chemical vapor deposition using acetylene as a carbon source. Milli-Q water was used throughout all experiments.

Synthesizing method

The experimental work was executed via two main steps; the first step comprises the GQDs synthesizing, while the second step is intended for decorating the surface of MWCNTs with different amounts of GQDs. MWCNTs have been synthesized through atmospheric chemical vapor deposition. The details regarding the synthesizing method of MWCNTs and GQDs can be found in previously published articles [25,26].

Synthesis of GQDs using pyrolysis method

The GQDs were obtained through the pyrolysis technique. In brief, 5 grams of $C_6H_8O_7$ has been melted in a ceramic crucible at $180^\circ C$ for 12 h, then allowed to cool naturally to room temperature. 1 M of NaOH solution was poured into the melted citric acid at this stage the color was changed to yellow. The resultant mixture was rinsed in deionized water and washed several times till neutralization, finally the powder dried at $80^\circ C$ overnight. The subsequent step comprises the attachment of GQDs externally to the outer surface of MWCNTs.

Synthesis of GQDs/CNTs nanocomposite with different ratios of GQDs

30 mg of MWCNTs were dispersed in 50 ml of H_2O using ultrasonic homogenized for 30 min. The amount of MWCNTs is fixed for different amounts of GQDs. Different loading ratios of 10%, 20%, and 30% of the pre-synthesized GQDs were added to the MWCNTs suspension. The MWCNTs and GQDs mixture was sonicated for 30 minutes, filtered, washed, and dried. The resultant composites were investigated using different characterization techniques. The schematic representation of the synthesizing method is reported in Figure 1.

Characterization techniques

The crystal structure and related structure parameters were identified and calculated using the X-ray diffraction (XRD) technique. The Malvern

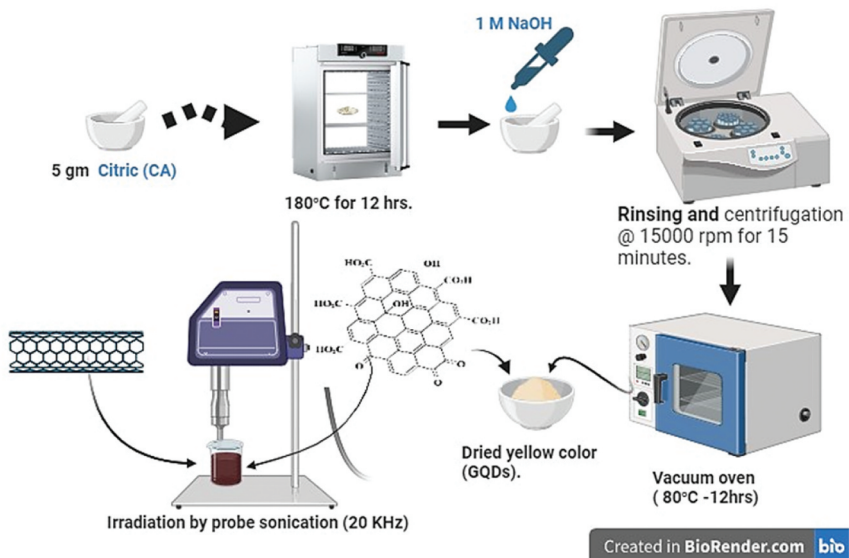


Figure 1. The schematic diagram of the synthesizing procedures of GQDs/CNTs.

Panalytical Empyrean 3 XRD diffractometer with Copper K α , from 5–90° was used to obtain XRD patterns. The morphological features and detailed microstructure were explored by a high-resolution transmission electron microscope (HR-TEM) (JEM 2100, JEOL HR-TEM microscope) operated at 200 KVA. The UV-Vis spectrum was acquired using Agilent Cary5000 in the spectral range from 200 to 800 cm⁻¹. The Raman bands of the studied composites were verified using a confocal Raman microscope (Witec Alpha 300 RA, 514 nm excitation). The BET surface area, average pore diameter, and pore volume were measured using BELSORPP MAX II.

CO₂ capture measurements

The CO₂ capacity of the prepared samples was evaluated using a chemisorption technique by the temperature-programmed desorption of carbon dioxide (CO₂) that was used to determine the amount and strength of the basic sites and the capacity of prepared samples to store the CO₂ gas. The catalyst (50 mg) was pre-treated at 200 °C under a stream of Helium gas (50 mL min⁻¹) for 2 h, then cooled down to 40 °C. After that, the CO₂ gas was introduced into the flow system for 30 min, followed by purging with Helium gas was flowed at 40 °C for 15 min to remove the physically adsorbed CO₂. After that, the sample was heated at a rate of 10 °C/min up to 1000 °C, to desorb the stored CO₂ gas into the samples, the data were recorded by thermal conductivity detector (TCD). The amount of desorbed CO₂ gas was calculated by the area under the curves and compared with the standard gas sample.

Results and discussion

The XRD patterns of the as-prepared nanomaterials are depicted in [Figure 2](#). The XRD pattern of MWCNTs ([Figure 2a](#)) demonstrates a main diffraction peak

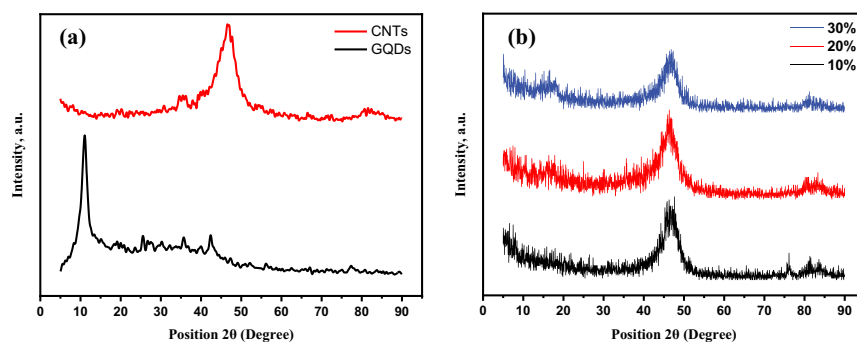


Figure 2. The XRD pattern of the synthesized materials, a) CNTs and GQDs and b) GQDs/CNTs composite.

at 45° corresponding to the (001) diffraction plane of MWCNTs. Furthermore, the diffraction pattern of GQDs (Figure 2a) has four diffraction peaks at 11°, 25°, 35°, and 42°, corresponding to (111), (400), (440), and (622) diffraction planes. The obtained pattern is in good agreement with standard card No. 01-082-2261. The XRD pattern of GQDs exhibited diffraction peaks at 25.57°, 35.65°, and 42.33° that can be indexed to the (111), (400), (440), and (622) which coincidence with card No. 01-082-2261 [25]. The broadness of the main diffraction peaks is characteristic of the small sizes of the GQDs. The estimated crystallite size of GQDs (from Deby – Scherrer) was about 2 nm. The three measured patterns of CNTs/GQDs (Figure 2b) have a broad diffraction peak at 43° corresponding to (001) of carbon nanotubes in addition to a less intense peak at approximately 15° that confirms the presence of GQDs in the prepared composites. The intensity of the minor peak increases as the amount of the GQDs increases. Some related structural parameters were calculated to get more information regarding the crystal structure of the prepared samples. The calculated parameters represented in Table 1 are crystallite size (D), lattice strain (ϵ), inter-planar distance (d), dislocation density (δ), number of crystallite sizes per unit area (N), and distortion parameters (g). The stated parameters were calculated using the following formula [25,27,28]:

$$D = \left[\frac{(k) \times (\lambda)}{(\beta_D) \times (\text{Cos}\theta)} \right] \quad [1]$$

$$\epsilon = \left\{ \frac{\beta_D}{4 \times \sin\theta} \right\} \quad [2]$$

$$d = \frac{\lambda}{2 \sin \theta} \quad [3]$$

$$\delta = \left\{ \frac{1}{D^2} \right\} \quad [4]$$

$$N = \frac{d}{D^2} \quad [5]$$

$$g = \frac{\beta}{\tan \theta} \quad [6]$$

Table 1. The calculated structure parameters of the synthesized structures.

Sample	D (nm)	d-spacing (Å)	ϵ	δ (nm ⁻²)	N	g
10%	26.55051	0.19062	0.003231	0.001419	0.00027	0.012923
20%	6.83408	0.195739	0.012889	0.021411	0.004191	0.051555
30%	5.471397	0.193843	0.015943	0.033404	0.006475	0.063771

Where λ is the wavelength for the X-ray source (CuK α), β represents the full width at the median of the highest value, and θ is the diffraction angle. The average crystallite size decreases as the amount of loaded GQDs increases. The distortion parameter, dislocation density, and lattice strain increase due to the incorporation of GQDs with MWCNTs. It is well known that the insertion of forging atoms or molecules increases the strain inside the host matrix. The number of crystallite size per unit area was also increased as the fraction of GQDs increased. This means that more particles are packaged in the same volume, and this seems to be logical as the amount of tiny GQDs increases with increasing concentration in the studied structures.

The HR-TEM has been utilized to elaborate detailed morphological features and particle size of the prepared nanocomposites. The selected area electron diffraction (SAED) was also captured to investigate the crystal structure of the sample. The HR-TEM of the 30% sample at different magnifications is illustrated in Figure 3.

The common morphological feature (Figure 3a) of the present captures reveals different two types of nanocarbon structures, carbon nanotubes and tinny spherical nanocarbon particles. The carbon nanotubes have a hollow tubular structure. It is composed of multi-concentrated tubes confirming the multiwall structure of the MWCNTs., furthermore, it reveals that the GQDs appear as minuscule particles attached externally to the outer surface of MWCNTs. The size of the GQDs was measured and found to be as low as 1 nm as demonstrated in Figure 3b, c. Some agglomeration was also observed, this could be due to the attached functional groups. The SAED of Figure 3d demonstrates concentrated continuous rings that confirm the polycrystalline structure of the prepared composite. The HR-TEM in conjunction with the XRD diffraction pattern confirms the successful incorporation of GQDs and MWCNTs.

The optical properties of the studied structures have been demonstrated using UV-Vis measurements in the spectral range of 200–800 nm as demonstrated in Figure 4. The UV-Vis spectra of MWCNTs displayed in Figure 4a showed an absorption peak at 250 nm. It was observed that the

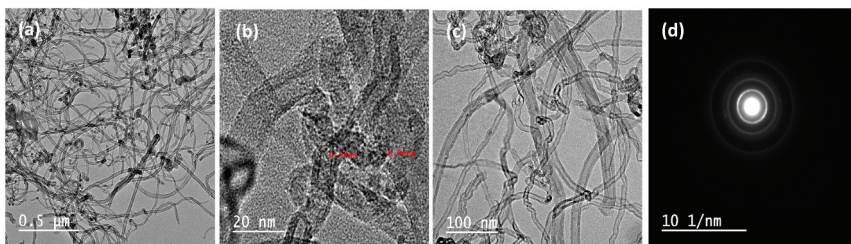


Figure 3. The HR-TEM of the sample 30% a), b), and c) at different magnifications, and d) SAED.

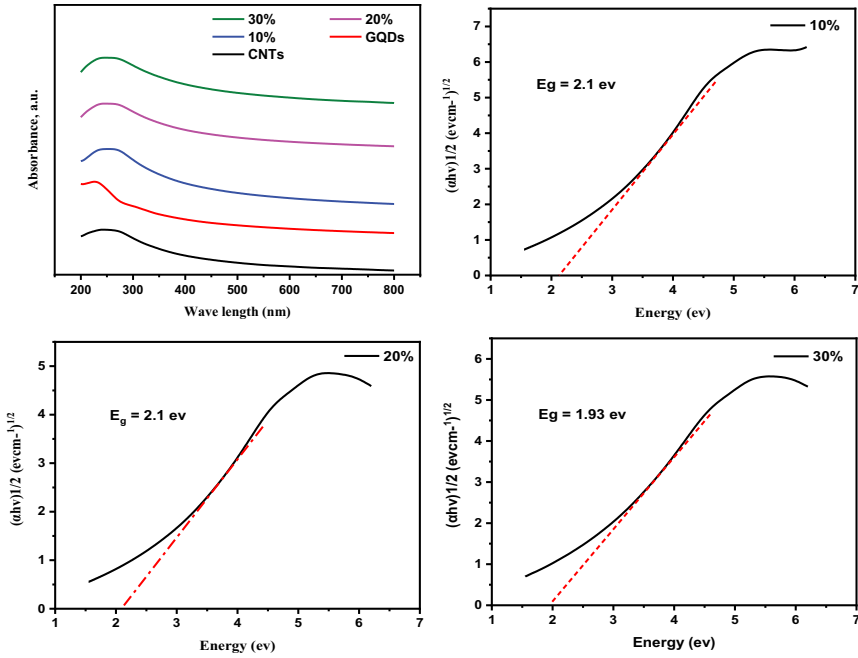


Figure 4. Optical properties of the synthesized nanomaterials and nanocomposites a) UV- Vis spectrum of all synthesized nanomaterials and nanocomposites, b) energy band gap of 10% sample, c) energy band gap of 20% sample, and d) energy band gap of 30% sample.

absorption band of MWCNTs is weak and that could be related to the bundling of nanotubes. It was reported that just segregated nanotubes have absorption peaks in the UV-Vis region, while the agglomerated carbon nanotubes have no peaks in the same region [29]. The absorption peak of MWCNTs in the UV-Vis region confirms the dispersibility of synthesized MWCNTs, as well as the absorption peak at 225 nm which confirms the presence of GQDs. This peak is related to the π - π^* transition of sp^2 domains in GQDs [30]. The UV-Vis absorption shoulder peak of GQDs at 225 nm was shifted to 260 nm after combining the CNTs and GQDs. This shift confirms the successful incorporation of GQDs and MWCNTs via π - π interaction. This interaction occurs between sp^2 hybridized regions of GQDs and the external surface of the MWCNTs [31]. The energy band gap was calculated from the UV-Vis spectra using the following Equation (equation 7):

$$\alpha h\nu = (h\nu - E_g)^2 \quad [7]$$

The E_g represents the energy band gap, α is the absorption coefficient, and h is devoted to the Plank's constant. The band gap energy is obtained from the tangent of the $(\alpha h\nu)^{1/2}$ and $h\nu$ plotting. The estimated band gap energies are 2.1 eV, 2.1 eV, and 1.93 eV for 10%, 20%, and 30% as shown in Figure 4b-d, respectively. It can be recognized that the band gap energy of 10% and 20% samples have the same value, while this value decreased for the 30% sample.

Raman spectroscopy is one of the most trusted tools for identifying nanocarbon-based materials. The Raman spectra of the synthesized materials were measured with the excitation laser source of 532 nm as shown in Figure 5. The obtained spectrum revealed three standard Raman shifts of D, G, and G' . The D band at 1340 cm^{-1} is due to the disordered active Raman mode. The G band at 1570 cm^{-1} originated from the stretching vibration of the in-plane mode (E_{2g}) band [32]. The third G' band at 2666 cm^{-1} represents the second mode of vibrations in the carbon atoms [33,34]. The origin of the G' band is attributed to the backscatter phonons and a scarce imperfection such as twisting, corrugation, and edges [35]. The most interesting value that can be deduced from the Raman spectrum is the I_D/I_G ratio. This ratio is commonly represented as a key factor for estimating the functionalization degree of nanomaterials. From another point of view, the I_D/I_G ratio is equivalent to SP^3/SP^2 , where the G band is not influenced by the presence of defects, while the D-band is promoted by the existence of sp^3 defects [36]. The estimated values for I_D/I_G were 0.89, 0.93, and 0.95 for 10%, 20%, and 30% samples, respectively. The I_D/I_G value increases as the amount of GQDs increases, which could be an indication of increasing the defects. These defects act as active sites for adsorbing CO_2 molecules.

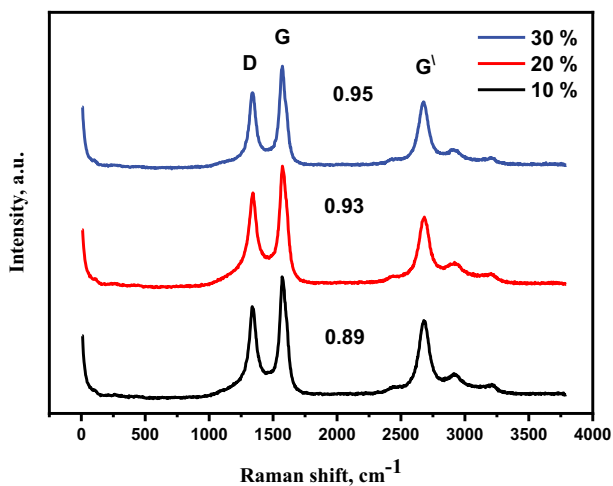


Figure 5. The Raman spectrum of 10%, 20%, and 30% samples.

Nitrogen adsorption–desorption isotherms were used to calculate the BET-specific surface area and pore size distribution in the CNTs and GQDs/CNTs nanocomposites, which are illustrated in Figure 6. It is interesting to note that all isotherms belong to the type III b isotherm with H3 hysteresis loops as (BDDT classification) [37]. The apparent hysteresis loop in the relative pressure range of 0.9–1.0 indicates that the adsorption is associated with semi-filled pores in multilayer or macroporous particles [38].

The calculated BET and average pore diameter parameters for each sample are listed in Table 2. It is noteworthy that the calculated BET decreased with an increase in the GQDs ratio; it is also the average pore diameter and pore

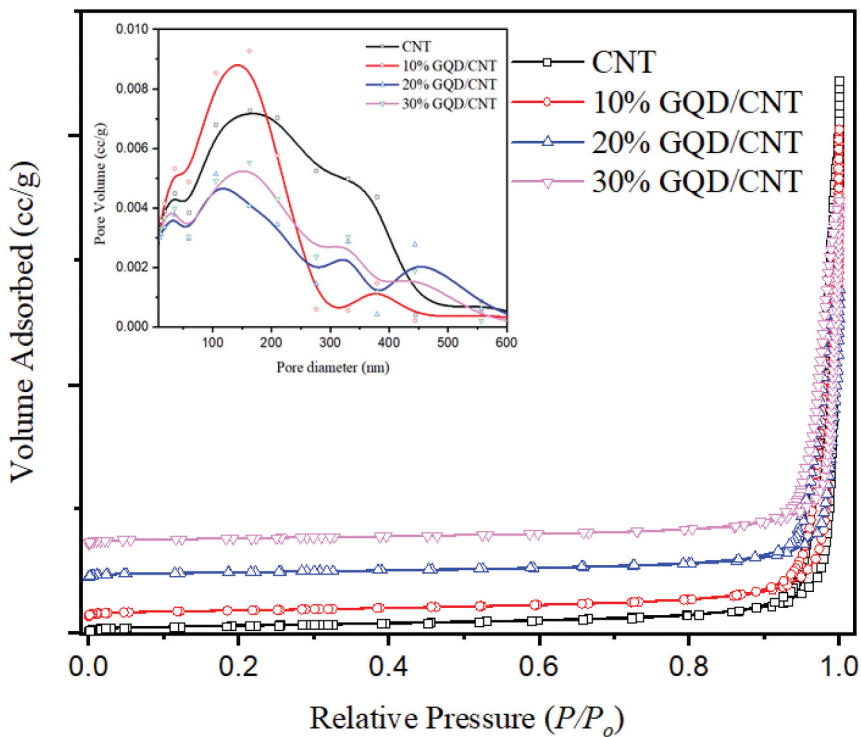


Figure 6. Adsorption-desorption isotherm of CNTs and its composites with GQDs (inset) pore size distribution.

Table 2. Specific surface areas and pore structures of as-synthesized CNTs and their composites.

Sample	Surface area m^2/g	Average pore diameter. nm	pore volume $\text{cm}^3 \text{g}^{-1}$
CNT	114.4	75.9	2.49
10% GQDs/CNTs	109.4	56.5	1.90
20% GQDs/CNTs	86.8	49.6	1.45
30% GQDs/CNTs	96.5	52.3	1.56

volume that decreased with an increase in the GQDs ratio that indicates the GQDs blocked the cylindrical tube of MWCNTs [39] that corresponded with the TEM view.

To measure the ability of samples to trap CO₂ gas, they should be exposed to the flow rate of CO₂ gas under a temperature-programmed desorption system. The CO₂ capture test was carried out by pretreatment of samples using He gas (30 ml min⁻¹) with an increase in temperature up to 200°C for 2 h to remove any adsorbed gas on the sample's surface [40]. After that, the samples were cooled to 40 °C, then the CO₂ gas was loaded with a flow rate of 30 mL/min for 30 min, and then the saturated powder samples were purged with He (30 mL/min) for 15 min to remove residual or physisorbed CO₂ on the surface of the samples. The CO₂ gas that was captured into the sample by the chemisorption mechanism was determined by increasing the temperature to 1000 °C at a heating rate of 10 °C/min. The volume of CO₂ that was desorbed has been determined using a thermal conductivity detector (TCD). The amount of CO₂ desorbed was calculated by integrating the TPD curves, which reveal that the capacity of the CO₂ capture increased with an increase in the GQDs in the samples.

The amounts of CO₂ adsorbed into the sample are 2, 8.3, 24, and 25 mmol. g⁻¹ for pristine CNTs, 10% GQD/CNT, 20% GQD/CNT, and 30% GQD/CNTs, respectively, as shown in Figure 7. Table 3 shows the amount of captured CO₂ gas and the comparison with the surface area and basic sites density [41]. The table values and Figure 8 revealed

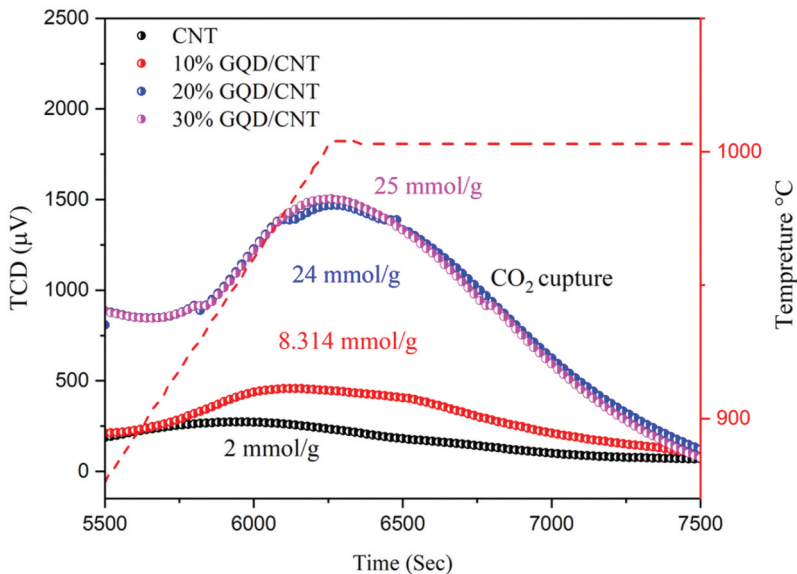
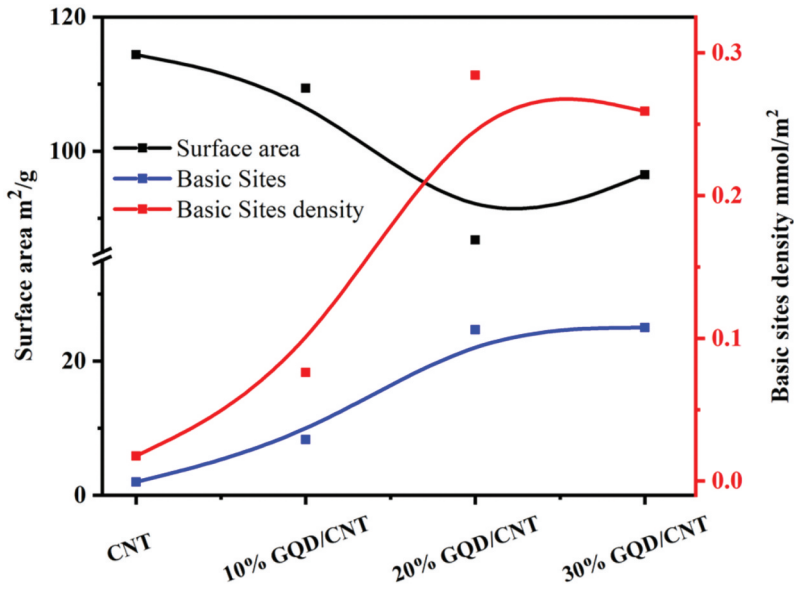


Figure 7. CO₂-TPD profiles of CNTs and its composites.

Table 3. CO₂-TPD data of as-synthesized CNTs and its composites.

sample	CO ₂ desorption peak area	CO ₂ mmol/g	S A m ² /g	Basic sites density
CNTs	170,186	2	114.4	0.017
10% GQD/CNTs	707464	8.314	109.4	0.075
20% GQD/CNTs	2047957	24.666	86.8	0.28
30% GQD/CNTs	2127482	25.001	96.5	0.25

**Figure 8.** Summary comparison for CNT and its composites using SA, basic sites, and basic sites' density.

that the 20% GQDs/CNTs and 30% GQDs/CNTs showed the lowest value of the surface area and average pore diameter. Furthermore, the 30% GQDs/CNTs and 20% GQDs/CNTs showed the best performance for the CO₂ gas capture of about 25 mmol. g⁻¹ and 24.6 mmol. g⁻¹. This results due to the increase of the active site density on the surfaces of 20% and 30 % GQDs/CNTs compared to the other samples. Also, due to the small pore diameter, the desorption peaks occurred at high temperatures.

Conclusion

In this study, the effect of the loading ratio of GQDs in the GQDs/CNTs nanocomposite was investigated on the CO₂ capture. Therefore, different amounts of GDQs (10%, 20%, and 30%) were loaded on the surface of Multiwalled carbon nanotubes via ultrasonication method. The properties

of the resultant structures were investigated through XRD, HR-TEM, UV-Vis, Raman and BET analysis. The XRD patterns of the samples confirm the presence of the GQDs and the CNTs, as well as the average crystallite size decreases as the amount of loaded GQDs increases. The distortion parameter, dislocation density, and lattice strain increase due to the incorporation of GQDs with MWCNTs. The HR-TEM confirms that the GQDs are well incorporated in the CNTs, and this is also proved from the surface area and porosity of the samples, since the BET surface area, the average pore diameter, and the pore volume decreased with increasing the GQDs ratio indicate that the GQDs blocked the cylindrical tube of MWCNTs. The optical band gap was calculated for the nanocomposites, it was decreased upon increasing the ratio of the GQDs, since the 30% GQDs/CNT shows E_g of about 1.93 eV compared to 2.1 eV for the 10% and 20% GQDs/CNTs. The CO_2 capture of 24.6 mmol. g^{-1} and 25 mmol. g^{-1} was verified for 20% GQD/CNT and 30% GQD/CNT with basic site densities of 0.28 and 0.25, respectively, in addition to pore size diameters of 49.6 nm and 52.3 nm, respectively.

Disclosure statement

No potential conflict of interest was reported by the author(s).

ORCID

Mohamed Morsy  <http://orcid.org/0000-0002-0019-2773>

References

1. Rios-Saldaña LE, Sapag K, Nieto-Delgado C, et al. Enhancing the CO_2 capture capacity of natural macroporous carbonized fibers by growing carbon nanotubes on their surface. *Colloids Surf A Physicochem Eng Asp.* 2023;669:131524. doi: [10.1016/j.colsurfa.2023.131524](https://doi.org/10.1016/j.colsurfa.2023.131524)
2. Irani M, Jacobson AT, Gasem KAM, et al. Modified carbon nanotubes/tetraethylenepentamine for CO_2 capture. *Fuel.* 2017;206:10–18. doi: [10.1016/j.fuel.2017.05.087](https://doi.org/10.1016/j.fuel.2017.05.087)
3. Keller L, Ohs B, Abduly L, et al. Carbon nanotube silica composite hollow fibers impregnated with polyethylenimine for CO_2 capture. *Chem Eng J.* 2019;359:476–484. doi: [10.1016/j.cej.2018.11.100](https://doi.org/10.1016/j.cej.2018.11.100)
4. Wu F, Zhou Z, Temizel-Sekeryan S, et al. Assessing the environmental impact and payback of carbon nanotube supported CO_2 capture technologies using LCA methodology. *J Clean Prod.* 2020;270:122465. doi: [10.1016/j.jclepro.2020.122465](https://doi.org/10.1016/j.jclepro.2020.122465)
5. Zeng Y, Li K, Zhu Q, et al. Capture of CO_2 in carbon nanotube bundles supported with room-temperature ionic liquids: a molecular simulation study. *Chem Eng Sci.* 2018;192:94–102. doi: [10.1016/j.ces.2018.07.025](https://doi.org/10.1016/j.ces.2018.07.025)

6. Su F, Lu C, Chung A-J, et al. CO₂ capture with amine-loaded carbon nanotubes via a dual-column temperature/vacuum swing adsorption. *Appl Energy*. 2014;113:706–712. doi: [10.1016/j.apenergy.2013.08.001](https://doi.org/10.1016/j.apenergy.2013.08.001)
7. Zainab G, Iqbal N, Babar AA, et al. Free-standing, spider-web-like polyamide/carbon nanotube composite nanofibrous membrane impregnated with polyethyleneimine for CO₂ capture. *Compos Commun*. 2017;6:41–47. doi: [10.1016/j.coco.2017.09.001](https://doi.org/10.1016/j.coco.2017.09.001)
8. Keller L, Ohs B, Lenhart J, et al. High capacity polyethylenimine impregnated microtubes made of carbon nanotubes for CO₂ capture. *Carbon N Y*. 2018;126:338–345. doi: [10.1016/j.carbon.2017.10.023](https://doi.org/10.1016/j.carbon.2017.10.023)
9. Sun Q, Wang M, Li Z, et al. CO₂ capture and gas separation on boron carbon nanotubes. *Chem Phys Lett*. 2013;575:59–66. doi: [10.1016/j.cplett.2013.04.063](https://doi.org/10.1016/j.cplett.2013.04.063)
10. Su F, Lu C, Cnen W, et al. Capture of CO₂ from flue gas via multiwalled carbon nanotubes. *Sci Of The Total Environ*. 2009;407(8):3017–3023. doi: [10.1016/j.scitotenv.2009.01.007](https://doi.org/10.1016/j.scitotenv.2009.01.007)
11. Moustafa H, Ahmed EM, Morsy M. Bio-based antibacterial packaging from decorated bagasse papers with natural rosin and synthesised GO-Ag nanoparticles. *Mater Technol [Internet]*. 2022;37(13):2766–2776. Available from doi:[10.1080/10667857.2022.2074939](https://doi.org/10.1080/10667857.2022.2074939)
12. Eysa HM, Afifi M, Moustafa H. Improvement of the acoustic and mechanical properties of sponge ethylene propylene diene rubber/carbon nanotube composites crosslinked by subsequent sulphur and electron beam irradiation. *Polym Int*. 2022;72(1):87–98. doi: [10.1002/pi.6449](https://doi.org/10.1002/pi.6449)
13. Zhao P, Shen B, Wang J, et al. The production and electrochemical performance of carbon nano-materials derived from plastics over nickel-based catalysts with different supports. *Fuel Process Technol*. 2023;249:107853. doi: [10.1016/j.fuproc.2023.107853](https://doi.org/10.1016/j.fuproc.2023.107853)
14. Moustafa H, Isawi H, Abd El Wahab SM. Utilization of PVA nano-membrane based synthesized magnetic GO-Ni-Fe₂O₄ nanoparticles for removal of heavy metals from water resources. *Environ Nanotechnol Monit Manag [Internet]*. 2022;18:100696. Available from: <https://www.sciencedirect.com/science/article/pii/S2215153222000563>
15. Yuan J, Wang Y, Tang M, et al. Preparation of N, O co-doped carbon nanotubes and activated carbon composites with hierarchical porous structure for CO₂ adsorption by coal pyrolysis. *Fuel*. 2023;333:126465. doi: [10.1016/j.fuel.2022.126465](https://doi.org/10.1016/j.fuel.2022.126465)
16. Kang K, Liu B, Yue G, et al. Preparation of carbon quantum dots from ionic liquid modified biomass for the detection of Fe³⁺ and Pd²⁺ in environmental water. *Ecotoxicol Environ Saf*. 2023;255:114795. doi: [10.1016/j.ecoenv.2023.114795](https://doi.org/10.1016/j.ecoenv.2023.114795)
17. Tong S, Zhou J, Ding L, et al. Preparation of carbon quantum dots/TiO₂ composite and application for enhanced photodegradation of rhodamine B. *Colloids Surf A Physicochem Eng Asp*. 2022;648:129342. doi: [10.1016/j.colsurfa.2022.129342](https://doi.org/10.1016/j.colsurfa.2022.129342)
18. Wang C, Sun Q, Yang M, et al. Preparation of highly luminescent nitrogen-doped carbon quantum dots and their detection of tetracycline antibiotics. *Colloids Surf A Physicochem Eng Asp*. 2022;653:129982. doi: [10.1016/j.colsurfa.2022.129982](https://doi.org/10.1016/j.colsurfa.2022.129982)
19. Zheng J, Lian X, Wu M, et al. One-step preparation of Ni₃S₄ quantum dots composite graphene/carbon nanotube conductive network for asymmetric

- supercapacitor. *J Alloys Compd.* **2021**;859:158247. doi: [10.1016/j.jallcom.2020.158247](https://doi.org/10.1016/j.jallcom.2020.158247)
20. Guo L-P, Zhang Y, Li W-C. Sustainable microalgae for the simultaneous synthesis of carbon quantum dots for cellular imaging and porous carbon for CO₂ capture. *J Colloid Interface Sci.* **2017**;493:257–264. doi: [10.1016/j.jcis.2017.01.003](https://doi.org/10.1016/j.jcis.2017.01.003)
 21. Yang H-L, Bai L-F, Geng Z-R, et al. Carbon quantum dots: preparation, optical properties, and biomedical applications. *Mater Today Adv.* **2023**;18:100376. doi: [10.1016/j.mtadv.2023.100376](https://doi.org/10.1016/j.mtadv.2023.100376)
 22. Si Q-S, Guo W-Q, Wang H-Z, et al. Carbon quantum dots-based semiconductor preparation methods, applications and mechanisms in environmental contamination. *Chin Chem Lett.* **2020**;31(10):2556–2566. doi: [10.1016/j.ccllet.2020.08.036](https://doi.org/10.1016/j.ccllet.2020.08.036)
 23. Kondée S, Arayawut O, Pon-On W, et al. Nitrogen-doped carbon oxide quantum dots for flexible humidity sensor: experimental and SCC-DFTB study. *Vacuum.* **2022**;195:110648. doi: [10.1016/j.vacuum.2021.110648](https://doi.org/10.1016/j.vacuum.2021.110648)
 24. Yeh Y-J, Lin W, Chiang W-H, et al. Plasma-engineered graphene quantum dot-based nanocomposites as smart CO₂-philic membranes with extremely high separation performance. *Chem Eng J.* **2023**;476:146547. doi: [10.1016/j.cej.2023.146547](https://doi.org/10.1016/j.cej.2023.146547)
 25. Morsy M, Gomaa I, Mokhtar MM, et al. Design and implementation of humidity sensor based on carbon nitride modified with graphene quantum dots. *Sci Rep [Internet].* **2023**;13(1):1–18. Available from doi:[10.1038/s41598-023-29960-8](https://doi.org/10.1038/s41598-023-29960-8)
 26. Morsy M, Helal M, El-Okr M, et al. Preparation, purification and characterization of high purity multi-wall carbon nanotube. *Spectrochim Acta A Mol Biomol Spectrosc.* **2014**;132:594–598. doi: [10.1016/j.saa.2014.04.122](https://doi.org/10.1016/j.saa.2014.04.122)
 27. Waikar MR, Raste PM, Sonker RK, et al. Enhancement in NH₃ sensing performance of ZnO thin-film via gamma-irradiation. *J Alloys Compd.* **2020**;830:154641. doi: [10.1016/j.jallcom.2020.154641](https://doi.org/10.1016/j.jallcom.2020.154641)
 28. Waikar MR, Sonker RK, Gupta S, et al. Post- γ -irradiation effects on structural, optical and morphological properties of chemical vapour deposited MWCNTs. *Mater Sci Semicond Process.* **2020**;110:104975. doi: [10.1016/j.mssp.2020.104975](https://doi.org/10.1016/j.mssp.2020.104975)
 29. Sapalidis A, Sideratou Z, Panagiotaki KN, et al. Fabrication of antibacterial poly (vinyl alcohol) nanocomposite films containing dendritic polymer functionalized multi-walled carbon nanotubes. *Front Mater.* **2018**;5:1–10. doi: [10.3389/fmats.2018.00011](https://doi.org/10.3389/fmats.2018.00011)
 30. Wu W, Cao J, Zhong M, et al. Separating graphene quantum dots by lateral size through gel column chromatography. *RSC Adv.* **2019**;9(33):18898–18901. doi: [10.1039/C9RA03623G](https://doi.org/10.1039/C9RA03623G)
 31. Kavinkumar T, Synthesis MS. Characterization and gas sensing properties of graphene oxide- multi walled carbon nanotube composite journal of materials science & technology synthesis, characterization and gas sensing properties of graphene oxide-multiwalled carbon Nanotu. *J Mater Sci Technol.* **2016**;32(7):626–632. doi: [10.1016/j.jmst.2016.03.017](https://doi.org/10.1016/j.jmst.2016.03.017)
 32. Jayanthi S, Mukherjee A, Chatterjee K, et al. Tailored nitrogen dioxide sensing response of three-dimensional graphene foam. *Sens Actuators B Chem.* **2016**;222:21–27. doi: [10.1016/j.snb.2015.08.041](https://doi.org/10.1016/j.snb.2015.08.041)
 33. Hosseini MA, Zare H, Malekie S. Raman spectroscopy of electron irradiated multi-walled carbon nanotube for dosimetry purposes. *Radiat Phys And Chem.* **2023**;202:110535. doi: [10.1016/j.radphyschem.2022.110535](https://doi.org/10.1016/j.radphyschem.2022.110535)

34. Laurenzi S, Botti S, Rufoloni A, et al. Mapping the residual strain of carbon nanotubes in DWCNT/epoxy nanocomposites after tensile load using Raman microscopy. *Compos Commun.* 2020;21:100424. doi: [10.1016/j.coco.2020.100424](https://doi.org/10.1016/j.coco.2020.100424)
35. Kumar Mahato P, Choudhuri S, Kumar C, et al. Evaluation of crystal size present in graphene oxide quantum dots using optical and Raman spectroscopy. *Mater Today Proc.* 2023;80:668–673. doi: [10.1016/j.matpr.2022.11.066](https://doi.org/10.1016/j.matpr.2022.11.066)
36. Nxele SR, Nyokong T. Time-dependent characterization of graphene quantum dots and graphitic carbon nitride quantum dots synthesized by hydrothermal methods. *Diam Relat Mater.* 2022;121:108751. doi: [10.1016/j.diamond.2021.108751](https://doi.org/10.1016/j.diamond.2021.108751)
37. Bui TT, Nguyen DC, Hua SH, et al. Sonochemical preparation of a magnet-responsive Fe₃O₄@ZIF-8 adsorbent for efficient Cu²⁺ removal. *Nanomaterials.* 2022;12(5):753. doi: [10.3390/nano12050753](https://doi.org/10.3390/nano12050753)
38. Wang W, Liu P, Zhang M, et al. The pore structure of phosphoaluminate cement. *Open J Composite Mater.* 2012;2(03):104–112. doi: [10.4236/ojcm.2012.23012](https://doi.org/10.4236/ojcm.2012.23012)
39. Kh R, Ismail SM, Sh L, et al. Structural, magnetic, and optical properties of ZnFe₂O₄/RO (RO = CdO, NiO, Ga₂O₃, SnO₂, and TiO₂) nanocomposites. *J Mater Sci.* 2023;58(19):7948–7967. doi: [10.1007/s10853-023-08539-8](https://doi.org/10.1007/s10853-023-08539-8)
40. Helal A, Harraz FA, Ismail AA. One-step synthesis of heterojunction Cr₂O₃ nanoparticles decorated Bi₂S₃ nanorods with enhanced photocatalytic activity for mineralization of organic pollutants. *J Photochem Photobiol A Chem.* 2021;419:113468. doi: [10.1016/j.jphotochem.2021.113468](https://doi.org/10.1016/j.jphotochem.2021.113468)
41. Wang L, Gao Y, Luo J, et al. Highly efficient catalytic direct air capture of CO₂ using ampholytic amino acid sorbent with acid-base bi-functional 3D graphene catalyst. *Chem Eng J.* 2023;477:147120. doi: [10.1016/j.cej.2023.147120](https://doi.org/10.1016/j.cej.2023.147120)